

# Spectral origin of non-Markovian open-system dynamics: A finite harmonic model without approximations

Ruggero Vasile,<sup>\*</sup> Fernando Galve,<sup>†</sup> and Roberta Zambrini<sup>‡</sup>

*IFISC (UIB-CSIC), Instituto de Física Interdisciplinary Sistemas Complejos, UIB Campus, 07122 Palma de Mallorca, Spain*

(Received 12 November 2013; published 14 February 2014)

Dissipation caused by nonhomogeneous bosonic finite chain environments (implementable in, e.g., segmented ion traps) is investigated through an exact diagonalization approach, avoiding common approximations used to describe open systems. Different spectral densities, including band gaps, can be engineered to separately assess different factors leading to memory effects, namely, the environment's size, temperature, proximity of the cutoff frequency, the spectral density's shape (sub-Ohmic, Ohmic, super-Ohmic), and the strength of its coupling to the system. Non-Markovianity is quantified with two recently introduced measures related to information backflow and nondivisibility of the system dynamical map. By sweeping the bath spectrum via tuning of the system frequency we show strongest memory effects at band-gap edges and provide an interpretation based on energy flow between system and environment. A system weakly coupled to a stiff chain ensures a Markovian dynamics, while the size of the environment as well as the local density of modes are not substantial factors. We show an opposite effect when increasing the temperature inside or outside the spectral band gap. Further, non-Markovianity arises for larger (negative and positive) powers of algebraic spectral densities, being the Ohmic case not always the most Markovian one.

DOI: [10.1103/PhysRevA.89.022109](https://doi.org/10.1103/PhysRevA.89.022109)

PACS number(s): 03.65.Yz, 42.50.Lc, 42.70.Qs

## I. INTRODUCTION

Achievements in preparation, control, and measurements of quantum systems require a deep understanding of the mechanism of interaction between a given open quantum system and the surrounding environment [1]. From a theoretical point of view, popular approaches, e.g., derivations of master or quantum Langevin equations [1,2], are based on the assumption of an infinite heat bath with some given spectral density  $J(\omega)$  embedding all information about the real couplings and frequencies in the complex environment, and the structure of the coupling to the system. Typical approximations to simplify the treatment, such as negligible memory effects (Markovian approximation), system time coarse graining, weak system-bath coupling, large frequency cutoff, and Ohmic spectral density, drastically constrain the possible frequency dependence of  $J(\omega)$ . Although simplified spectral densities allow an analytical treatment, important deviations from these simple instances are common in several systems such as, for instance, electric circuits, acoustic polarons in metals and semiconductors, radiation damping of charged particles [1], photonic crystals [3–6], but also in ion traps suffering electric field noise [7], micromechanical oscillators [8], or polarized photons for broad frequency spectra [9].

Memory effects and deviations from Markovian dynamics have been widely explored considering the time dependence of master equation coefficients and deviations from exponential decays [1,10–12] but only in the last few years several approaches have been proposed to systematically distinguish Markovian evolution in terms of properties of the dynamical map [13–16]. Different measures allow one to quantify non-Markovianity (NM) in terms of deviations from the Lindblad

form of the generator of the master equation [13], backflow of information from the environment [14], and entanglement decay with an ancilla [15], to mention some of them. The recent endeavor to better characterize memory effects in open systems not only aims to a deeper understanding of dissipative dynamics in physical, biological, and chemical systems, but is also explored as a resource in quantum technologies [17].

The aim of this work is to identify non-Markovian effects originating in the structure of the system and bath couplings as well as in the distribution of energies, as given by the form of the spectral density  $J(\omega)$ . To this end we consider a microscopic model given by an inhomogeneous harmonic chain, avoiding the limitations of approximate approaches. Finite models of coupled oscillators have been used to assess entanglement dynamics [18] and its generation when attaching ions to a chain [19,20] and can also provide an insightful test bed to establish the regimes of validity of approximated master equations [21]. The case of an oscillator attached to a homogeneous chain was already studied by Rubin to determine the statistical properties of crystals with defects: This configuration leads to an Ohmic spectral density (thus Markovian, at least for large temperature) [22]. Moving to nonhomogeneous chain configurations, we inquire the origin of NM to distinguish among several independent features quantifying separately different sources of NM. When focusing on periodic systems (e.g., dimers), we can engineer spectral densities with finite band gaps, like in semiconductors or photonic crystals [3–5,23]. For suitable couplings we show that the system is actually influenced by the resonant portion of the environment. Memory effects [14,15] are then evaluated by sweeping the spectral density for a structured bath allowing us to show the effects of the local form of the spectrum.

Before introducing the model, we point out that experimental implementation of a tunable chain of oscillators can be obtained through recent progress in segmented Paul traps [24,25] also allowing tunability of ions couplings and on-site potentials. Other possible setups are based on photonic crystal

<sup>\*</sup>ruggero@ifisc.uib-csic.es

<sup>†</sup>fernando@ifisc.uib-csic.es

<sup>‡</sup>roberta@ifisc.uib-csic.es

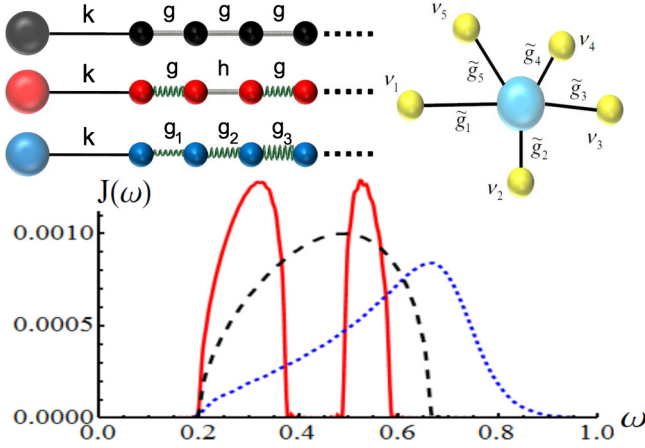


FIG. 1. (Color online) Examples of spectral densities which can be generated in our model: Rubin chain with  $g = 0.1$  and  $k = 0.01$  (black dashed line), gapped spectral density with  $g = 0.1$ ,  $h = 0.05$ , and  $k = 0.0075$  (red continuous line), and increasing coupling density with  $g_i = 0.1 + 0.05i$  and  $k = 0.01$  (blue dotted line); all cases with  $N = 200$  oscillators. Bath local potential frequency  $\omega_0 = 0.2$ . Couplings and frequencies are specified relative to a fixed (arbitrary) frequency unit, with  $\hbar = m = 1$ , in this and following figures. Schematic for the three plotted examples (top left) and of a star configuration (top right) also represented.

nanocavities, microtoroid resonators (see [26] for a review), or optomechanic resonators [27]. Furthermore, correlations spectra of the system can be measured to gain insight on the spectral density induced by the rest of the chain (see [8,10]). The nonhomogeneous harmonic chain we consider in this work represents then a structured and controllable reservoir amenable to experimental realization.

## II. THE MODEL: NONHOMOGENEOUS CHAIN

We consider an open quantum system consisting of a harmonic oscillator  $H_S = (p_S^2 + \omega_S^2 q_S^2)/2$ , where  $p_S$  and  $q_S$  are the system momentum and position operators, interacting with an environment ( $E$ ) that consists of  $N$  harmonic oscillators of frequency  $\omega_0$ , each interacting with its nearest neighbors with a springlike coupling of strength  $g_i$ . A particularly dramatic deviation from the Ohmic spectrum obtained with a homogeneous chain (Rubin model [22],  $g_i = g, \forall i$ ) is found when considering a periodic configuration (dimer) of identical oscillators with alternate values of couplings  $g$  and  $h \leq g$  (see Fig. 1):

$$H_E = \sum_i (p_i^2 + \Omega_i^2 q_i^2)/2 - g \sum_{i \text{ odd}} q_i q_{i+1} - h \sum_{i \text{ even}} q_i q_{i+1} \quad (1)$$

with  $\Omega_i = \sqrt{\omega_0^2 + h + g}$  ( $i = 2, \dots, N-1$ ) and  $\Omega_1 = \Omega_N = \sqrt{\omega_0^2 + g}$  [28]. For any  $\omega_0$  and  $g \neq h$  we build a band-gap model, characterized by a frequency spectrum distributed in an acoustic and an optical band separated by a finite gap [23]. The system is attached to the first element of the  $E$  chain and  $k$  is a coupling constant with an interaction term of the form  $H_I = -k q_S q_1$ . We consider a total initial factorized state  $\rho = \rho_S \otimes \rho$ , where  $\rho_S$  is a vacuum squeezed state and the chain environment is a Gibbs thermal state of temperature  $T$ ,  $\rho_E =$

$\exp(-H_E/k_B T)/Z$ . The chain configuration for real oscillators is mapped by diagonalization of the environment (through an orthogonal transformation  $\mathbf{K}$ ) into a star configuration of independent oscillators (bath's eigenmodes) of frequency  $\nu_i$  interacting with the system with strength  $\tilde{g}_i = k \mathbf{K}_{1i}$  (see Fig. 1 and Appendix A). In this work we will use units as referred to an arbitrary, but fixed, frequency unit. Couplings, times, and temperatures will be given in terms of this unit.

### A. Langevin equation

The reduced dynamics of the system is governed by a generalized Langevin equation, typically derived starting from a star environment [1,2],

$$\ddot{q}_S + \tilde{\omega}_S^2 q_S + \int_0^t ds \gamma(t-s) \dot{q}_S = \xi(t), \quad (2)$$

where  $\xi(t)$  is Langevin forcing of the system  $\xi(t) = \sum_i \tilde{g}_i [q_i \cos(\nu_i t) + p_i/\nu_i \sin(\nu_i t)] - \gamma(t) q_S(0)$ , and

$$\gamma(t) = \sum_i (\tilde{g}_i^2/\nu_i^2) \cos(\nu_i t) \quad (3)$$

is the damping kernel accounting for dissipation and memory effects and  $\tilde{\omega}_S$  is the system frequency after renormalization [1,2]. The spectral density can be obtained from the damping kernel as

$$J(\omega) = \omega \int_0^\infty \gamma(t) \cos(\omega t) dt. \quad (4)$$

For a finite number  $N$  of normal modes, the dissipative dynamics suffers recurrence for times  $\tau_R$  (related to reflection into the system of the fastest signals traveling along the chain), whose value depends on the number of modes  $N$  and on the frequency spectrum [29]. If we look at times  $t < \tau_R$  the spectral density (4) can be described by a smooth function of frequency. The form of this function can be directly related to the dynamical properties of the system. For instance, a linear—Ohmic—spectral density, i.e.,  $J(\omega) \propto \omega$ , leads to a Markovian equation with time-independent friction kernel  $-\gamma_0 \dot{q}(t)$ . In the Rubin model (i.e., the upper uniform chain in Fig. 1 when  $N \rightarrow \infty$ ) it is possible to show that  $J(\omega) \propto k \sqrt{\omega^2 - \omega_0^2} \sqrt{\omega_c^2 - \omega^2}$  with  $\omega_c = \sqrt{2g}$  the highest (cutoff) frequency in the spectrum of normal modes. When the on-site potential is absent ( $\omega_0 = 0$ ) and the system frequency is small compared to the cutoff, the Rubin model reproduces the Ohmic condition  $J(\omega) \propto \omega$  [1]. Other nonhomogeneous chain examples are shown in Fig. 1 with their respective spectral densities.

## III. RESONANCE CONDITIONS

In order to investigate the role of the spectral density's shape, we first need to know to what extent the system is affected by different bath eigenmodes depending on their relative detuning. To do so we compare the state of the system  $\rho(t)$  with  $\rho_\delta(t)$  obtained by allowing the system to interact only with those normal modes whose frequencies lie within a range  $\delta$  to system frequency  $\omega_S$ , i.e., such that  $|\nu_i - \omega_S| < \delta$ . The time evolution is obtained by a full diagonalization of  $H_S + H_E + H_I$  (see Appendix B). Deviation between  $\rho(t)$

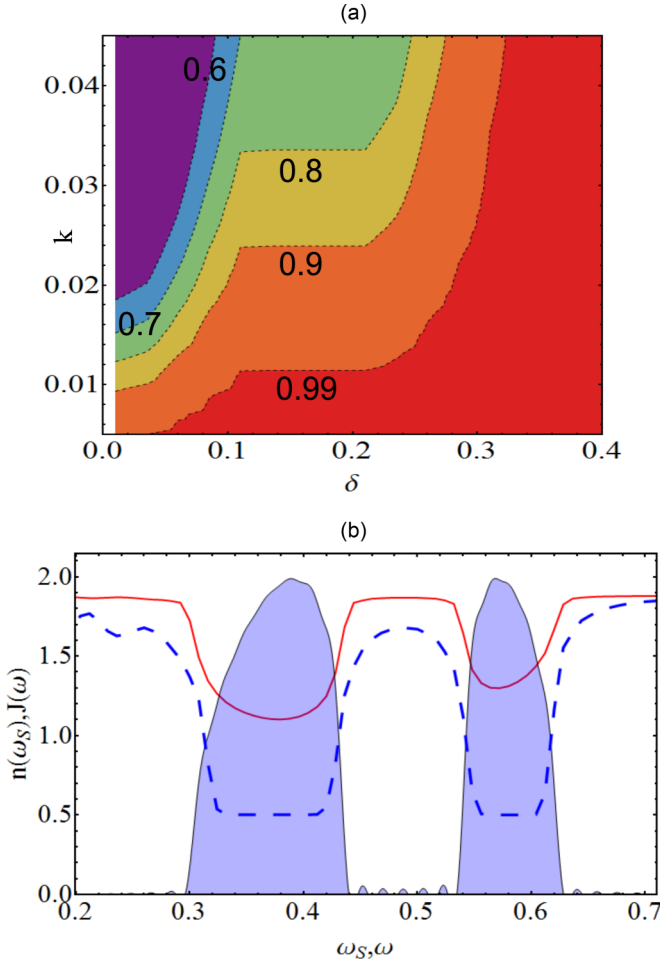


FIG. 2. (Color online) (a) Averaged fidelity as a function of system-bath coupling  $k$  and bandwidth  $\delta$ , for a band-gap density [shaded area in (b)] with  $g = 0.1$ ,  $h = 0.05$ ,  $\omega_0 = 0.3$ , and  $\omega_S = 0.65$  at temperature  $T = 0$ . Integration performed up to  $\tau_F = 400$  for  $N = 50$  oscillators. (b) System excitation number  $n = \langle H_S(\tau_F) \rangle / \omega_S$  at  $\tau_F = 400$  as a function of the system frequency  $\omega_S$  for a band-gap model with  $g = 0.1$ ,  $h = 0.05$ , and  $\omega_0 = 0.3$  [ $J(\omega)$  as shaded area] at  $T = 0$ . System-bath coupling  $k = 0.005$  (red solid) and  $k = 0.025$  (blue dashed). (Arbitrary units as specified in the caption of Fig. 1.)

and  $\rho_\delta(t)$  can be witnessed by the Uhlmann fidelity measure [30],  $\mathbf{F}(\rho, \rho_\delta) = \text{Tr} \sqrt{\sqrt{\rho} \rho_\delta \sqrt{\rho}}$ . This quantity averaged in time,  $\int_0^{\tau_F} \mathbf{F}(\rho, \rho_\delta) dt / \tau_F$ , is shown in Fig. 2(a) for a band-gap model with system frequency larger than the optical band,  $\omega_S > \omega_c$ . Here and in the following we choose  $\tau_F < \tau_R$  but big enough to explore the dissipative dynamics. If we take the value 0.99 as a guide for the eye, a weakly coupled oscillator ( $k < 0.01$ ) interacts only with a small vicinity of modes in the nearest band [right (optical) band in Fig. 1], while already for  $k = 0.012$  we need to take into account modes in the furthest band [left (acoustic) band]. This rough estimation allows one to appreciate that for weak couplings  $k \ll \omega_c$  a reduced number of resonant bath modes suffice to determine the system evolution.

The effect of the environment band gap is clearly shown by looking at the system excitation (average energy normalized by its frequency)  $n = \langle H_S(\tau_F) \rangle / \omega_S$  at  $\tau_F$  by varying the system frequency  $\omega_S$  to sweep the spectral density [Fig. 2(b)]. Energy

is dissipated continuously when  $\omega_S$  is resonant with the bath while it cannot propagate into the chain for  $\omega_S$  within the band gap (leading to oscillatory behavior and the formation of bound dressed states) [3,4,23,31].

#### IV. NON-MARKOVIAN DYNAMICS

Among the different quantifiers of NM appearing recently in the literature we consider hereafter the Breuer-Laine-Piilo (BLP) [14] and Rivas-Huelga-Plenio (RHP) [15] measures. The first (BLP) gives an interpretation of NM in terms of a backflow of information from the environment into the system. Its definition exploits the contractivity property of the quantum trace distance  $\mathbf{D}$  under completely positive and trace preserving maps. The lack of contractivity is a signature of the map nondivisibility and non-Markovianity [14]. For continuous variable systems, and within Gaussian states, the definition has been extended by substituting the trace distance with the fidelity  $\mathbf{F}$  [32,33], and the associated measure for the degree of NM reads

$$\mathbf{M}_{\text{BLP}} = \max_{\rho_1, \rho_2} \int_{dF/dt < 0} \frac{dF(\rho_1, \rho_2)}{dt} dt, \quad (5)$$

where the maximization is taken among all pairs of Gaussian states ( $\rho_1, \rho_2$ ) and integration is performed up to  $\tau_F$ .

The RHP criterion witnesses the nondivisibility of the dynamical map by preparing the system in an entangled state with an ancilla and evaluating the nonmonotonic time evolution of the entanglement. The measure reads [15]

$$\mathbf{M}_{\text{RHP}} = \int_0^{\tau_R} \left| \frac{dE_{SA}}{dt} \right| dt + E_{SA}(\tau_R) - E_{SA}(0), \quad (6)$$

where  $E_{SA}(t)$  denotes a proper system-ancilla entanglement measure, such as logarithmic negativity. This measure is based on the fact that local trace-preserving completely positive (CP) maps do not increase entanglement, hence any increase of entanglement at some time means that in such interval the dynamical map cannot be written as the composition of CP maps and nondivisibility characterizes non-Markovian dynamics (see [15] for a more detailed explanation). We should stress that when Eq. (6) gives zero, the map can be either divisible or nondivisible, i.e., it could still be non-Markovian, thus in these cases the measure is inconclusive. For details on the numerical evaluation of these two measures we refer the reader to Appendix C.

In Fig. 3 we show both NM measures for a dimer chain environment as a function of the system frequency  $\omega_S$  for temperature  $T = 0$ . We find that local NM maxima are present at the edges of the band-gap spectral density for both measures, while rapidly decreasing both inside the band and the gaps of the spectral density, at different rates. Sharp changes in frequency lead to long times in the Fourier transform, and are responsible for broad noise and dissipation kernels, for long time bath correlations [1,21], and for pronounced NM signatures, Fig. 3. Full Markovian behavior is achieved only inside the band where  $\mathbf{M}_{\text{BLP}} \sim 0$ . Even if the null value of the RHP measure is inconclusive, we note that increasing the system-bath coupling  $k$ , it raises to finite values, yielding a shape very much in agreement with the BLP measure. This is one of the few comparisons of two different NM measures in the literature [34].

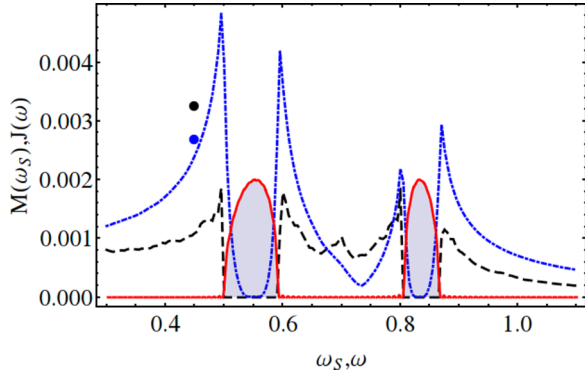


FIG. 3. (Color online) BLP non-Markovianity [blue (dot-dashed)] and RHP [black (dashed)] for  $N = 40$  oscillators,  $g = 0.2$ ,  $h = 0.05$ ,  $k = 0.001$ ,  $\omega_0 = 0.5$  when  $\omega_S$  is swept, for  $T = 0$ . The red (continuous) curve represents the spectral density function used in arbitrary units. The extra dots are evaluated at  $\omega_S = 0.45$  increasing the two-mode squeezing parameter from  $r = 1$  to 1.5 (for RHP NM, upper dot) and increasing the squeezing parameter range for the BLP NM (lower dot) maximization (from  $r \in \{0.5, 1\}$  to  $r \in \{0.125, 1.125\}$ ) (see Appendix C). (Arbitrary units as specified in the caption of Fig. 1.)

We also notice that in correspondence with the edges of the spectral density  $J(\omega)$ , where  $M_{\text{BLP}}$  is larger, we find a higher density of modes (i.e., there is an increasing number of eigenfrequencies when approaching the edge of the band gap). To exclude its connection with NM effects, we artificially engineered the spectral density to obtain a constant density of modes throughout the spectrum. This can be done considering a star model (see below) with equally spaced  $\nu_i$  frequencies within the bands. This allows us to establish that the enhancement of NM at the edges is actually not related to the normal mode density of states. The origin of NM is elsewhere.

Interaction between system and environment ( $H_I$ ) leads to energy exchange. When the system is in resonance with a band of the spectral density (optical or acoustical), energy is exchanged with many normal modes. In the real chain picture this corresponds to energy allowed to travel along the chain. This leads to an ever increasing indistinguishability of the states in Eq. (5) (all losing energy and relaxing) and thus to a zero (or close to zero) value of NM. On the other hand, at the band edges and in the band gaps, the energy lost by the system cannot travel freely along the chain, but bounces back and forth from the first elements of the chain to the system. This implies a periodical increase and decrease of distinguishability of the states whose fidelity we are integrating, hence we witness a higher NM value. The higher the detuning (deeper in the band gap), the less excitations and energy are exchanged, resulting in a diminishing value for the BLP NM. This result is in accordance with Ref. [10], where they study a generic (bosonic or fermionic) reservoir, and show that band gaps generate localized modes (thus dissipationless oscillatory behavior) plus nonexponential decays (identified there with NM). According to Ref. [14], Fig. 3 provides a quantitative measure of NM at band-gap edges as backflow of information.

## V. WHAT MAKES A BATH MARKOVIAN?

Besides the resonance conditions and the back reflection of information and energy when the system is out of resonance with the bath, what are the main factors leading to more Markovian dynamics? We have tried to answer this question in a fivefold approach, namely, with respect to the bath's size, its temperature, the width of its spectral density, its shape (sub-Ohmic, Ohmic, super-Ohmic), and the strength of its coupling to the system.

It is known that at low temperatures, Markovian approximations are generally not valid [1] and nonexponential decays of the correlation functions do arise [11]. In Fig. 4 (left) we show that the backflow of information  $M_{\text{BLP}}$  is similarly present only at low temperatures [ $T \lesssim \omega_c$ , assuming  $k_B = \hbar = 1$ ] when the system is dissipating within a band of the spectral density. Surprisingly, when we move to a nonresonant configuration, with the frequency of the system in the band gap, NM is found to increase with temperature [Fig. 4 (middle)]. When increasing temperature to higher values a linear increase of NM is observed within the gap, while in the band  $M_{\text{BLP}}$  tends to vanish. A similar behavior is observed for the  $M_{\text{RHP}}$  measure, though when inside the band it is inconclusive as entanglement with ancilla is always decaying.

Most prominent NM effects are expected in the strong coupling regime between system and bath [1,11]: Indeed reduction to Markovian dynamics is provided by a decrease of the coupling, which reduces NM by two orders of magnitude by one order of magnitude decrease in coupling. For the  $M_{\text{RHP}}$  we see that it tends to zero very fast (remember that a zero value is inconclusive) [Fig. 4 (right)].

### A. Star model

Finally we built an artificial star model (Fig. 1, top right) with equally spaced frequencies  $\nu_i$  and with assigned couplings  $\tilde{g}_i$ . In this way we can engineer in our simulations any functional dependence of the spectral density [the converse procedure, i.e., specify a given  $J(\omega)$  and then find frequencies and couplings of a linear chain that can reproduce it, is specified in [35,36]]. This allows us to look, as common in the literature, at deviations from the Ohmic case. For instance, the case of a spin in a dephasing environment shows NM signatures in the super-Ohmic case [37]. Here we start considering a star model of oscillators with algebraic spectral density function and with lower and upper sharp frequencies cutoffs  $J(\omega) = k(\omega/\omega_S)^l \Theta(\omega - \omega_c) \Theta(\bar{\omega}_c - \omega)$  (with  $\Theta$  the step function). In Fig. 5 (left) we show  $M_{\text{BLP}}$  for fixed cutoffs at 0.25, 0.75 (similar results are obtained by enlarging this range). We consider both positive and negative algebraic forms (the latter reported in a recent experiment with optomechanical oscillators [8]) and observe an increase of NM in both cases when departing from  $l_{\text{min}} \sim 1/2, 1, 1.4, 2, 2.8$  at temperatures  $T = 0, 0.25, 0.5, 1, 2$  ( $T = 2$  not shown). Surprisingly, the lowest NM is achieved for  $l = 1/2$  at zero temperature, instead of  $l = 1$  (Ohmic case). For higher temperatures the lowest value is achieved for  $l = 1$  or a bit higher. Also, a bath with  $J(\omega) \sim 1/\omega^2$  is more non-Markovian than one with  $J(\omega) \sim \omega^2$ . We also stress that different scaling and constraints

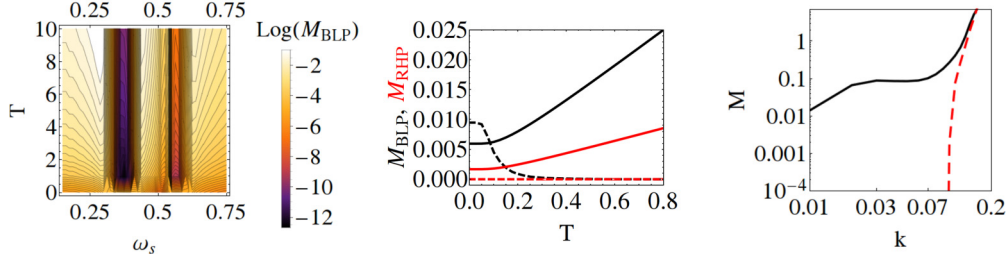


FIG. 4. (Color online) Left:  $\log(M_{\text{BLP}})$  for 50 oscillators,  $g = 0.1$ ,  $h = 0.05$ ,  $k = 0.001$ , and  $\omega_0 = 0.3$ , for temperatures  $T \in [0, 10]$  and  $\omega_s$  (the limits of the acoustic and optical bands are evident from the discontinuity of  $M_{\text{BLP}}$ ). Middle: Temperature dependence of  $M_{\text{BLP}}$  (black) and  $M_{\text{RHP}}$  [red (gray)] for  $\omega_s = 0.25(0.375)$  with continuous (dashed) line, i.e., out of (in) resonance. Right:  $M_{\text{BLP}}$  (continuous) and  $M_{\text{RHP}}$  (dashed) at  $\omega_s = 0.575$  for a homogeneous 50 oscillator (Rubin) chain,  $g = h = 0.1$  (i.e., no gap) and  $\omega_0 = 0.3$ . (Arbitrary units as specified in the caption of Fig. 1.)

of power function densities lead to significant influence on memory effects (see Appendix D).

The importance of frequency cutoff  $\omega_c$  in the spectral density is relevant not only to avoid unphysical divergences but also when discussing NM in terms of relevant time scales. A chain environment allows one to engineer the value of the frequency cutoff of an Ohmic environment by increasing the coupling strengths within the chain, however, this also changes the slope of  $J(\omega)$  at low  $\omega$ . In order to separately assess the role of the frequency cutoff, it is thus preferable to introduce artificial  $\tilde{g}_i$  in a star model to allow for the variation of  $\omega_c$  while keeping the initial slope of the spectral density (see the inset of Fig. 5, right). The result of such procedure is shown in Fig. 5 (right) where it is observed that an increase of  $\omega_c$  allows for a more monotonic flow of information into the environment leading to a decrease of NM.

We have also checked the dependence of NM with the bath size, seeing none (except for the role of the recurrence time). This is in accordance with the energy and information exchange conceptual relation that we have hypothesized; that

is, information (and energy) only flows back into the system when there is nonperfect resonance between the system and the bath. Whenever they are resonant, information and energy flow freely into the environment irrespective of its size.

## VI. CONCLUSIONS

We have considered different (nonphenomenological) spectral densities attainable by tuning nonhomogeneous oscillator chains that can be implemented in segmented ion chain traps and also with nanooscillators. A system attached at one extreme of the chain dissipates in this finite bath and exhibits memory effects. Its dynamics is analyzed considering continuous variables and Gaussian states. The importance of our analysis is the separate assessment, without approximations, of environment features that can be microscopically engineered and the quantitative comparison of two NM measures [14,15] to establish their influence in retaining environment memory effects. In spite of the difference between BLP and RHP measures, our analysis shows a good qualitative agreement on their dependence on different parameters whenever the second one is conclusive (i.e., not vanishing).

The possibility to tune the chain in a dimer configuration allows us to assess the influence of band gaps and to obtain a more detailed picture on the origin of Markovianity in relation to specific features of the spectral density. The main role describing the behavior of NM is played by a resonance condition: If the system is resonant with the normal modes of the bath, energy transfer along the chain is allowed and therefore information and energy flow irreversibly from system to bath leading to a Markovian dynamics. The largest backflow of information is found at the edges of the gaps where the energy bounces between the system and bath.

A high frequency cutoff and weak coupling, the first obtained by increasing the stiffness of the chain and the latter by decreasing the system-bath coupling, are major factors for ensuring Markovian dynamics. Indeed, NM effect of strong coupling or frequency cutoff, have already been discussed in the literature and we find consistent results. A relevant point when dealing with finite systems is that actually neither the size of the bath is important (only matters in limiting the recurrence time) nor the local density of modes has any significant influence on memory effects.

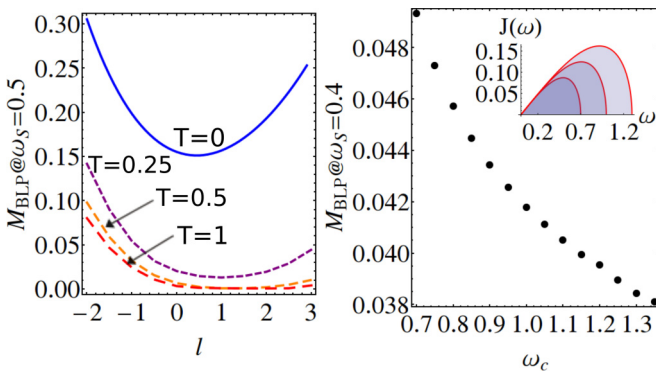


FIG. 5. (Color online)  $M_{\text{BLP}}$  for the star configuration with equally spaced eigenfrequencies, and couplings designed to give a specific  $J(\omega_s)$ . Left: spectral density function  $J(\omega) = k(\omega/\omega_s)^l \Theta(\omega - 0.25)\Theta(0.75 - \omega)$  ( $\Theta$  is the step function) is used. We show  $M_{\text{BLP}}$  as a function of  $l$  at  $\omega_s = 0.5$ , for temperatures  $T = 0, 0.25, 0.5, 1$ . Right: spectral density function  $J(\omega) = k\omega\sqrt{\omega_c^2 - \omega^2}/\omega_c$  is used with 40 oscillators and  $k = 0.00001$ . We plot  $M_{\text{BLP}}$  at  $\omega_s = 0.4$  when varying  $\omega_c$ . (Inset shows some of the  $J(\omega)$  functions corresponding to this situation; arbitrary units as specified in the caption of Fig. 1.)

On the other hand, unexpected results have been found when increasing temperature leading to opposite behavior inside and outside the band with a (linear in  $T$ ) NM increase in the band gap while inside the band memory effects become negligible for temperatures larger than the environment frequencies. Finally we have quantified NM when departing from the Ohmic case, considering positive and negative algebraic spectral densities  $J(\omega) \propto \omega^l$  for  $-2 \leq l \leq 3$  (being  $l = -2$  a recently measured value [8]) showing an enhancement of memory effects for both positive and negative values of  $l$ , with the Ohmic case ( $l = 1$ ) not being necessarily the most Markovian one.

The microscopic approach here adopted is useful not only to assess NM without approximations but also to have a deeper understanding of non-Markovian dynamics, looking at the energy flowing through the system. It would be interesting indeed to explore NM in more complex networks of oscillators [38] and also in different systems, such as qubits (see, for instance, the recent analysis in an homogeneous chain [39]).

#### ACKNOWLEDGMENTS

Financial support from MICINN, MINECO, CSIC, EU commission, FEDER funding under Grants No. FIS2007-60327 (FISICOS) and No. FIS2011-23526 (TIQS), postdoctoral JAE program (ESF), and COST Action MP1209 is acknowledged.

#### APPENDIX A: ENVIRONMENTAL DIAGONALIZATION

Let us consider the Hamiltonian  $H_E$  and rewrite it in the following way:

$$H_E = \frac{\mathbf{p}^T \mathbf{p}}{2} + \mathbf{q}^T \mathbf{A} \mathbf{q}, \quad (\text{A1})$$

where we compact the position and momentum operators in a vector formalism, i.e.,  $\mathbf{q} \equiv \{q_1, q_2, \dots, q_N\}^T$  and  $\mathbf{p} \equiv \{p_1, p_2, \dots, p_N\}^T$ . Moreover we have an  $N \times N$  matrix  $\mathbf{A}$  with elements  $A_{ij} = \Omega_i^2 \delta_{ij}/2 - G_{ij}/2$ , where the connection matrix  $\mathbf{G}$  has the following form:

$$\mathbf{G} = \begin{pmatrix} 0 & g & 0 & 0 & \dots & 0 \\ g & 0 & h & 0 & \dots & 0 \\ 0 & h & 0 & g & \dots & 0 \\ 0 & 0 & g & \dots & \dots & \dots \\ \dots & \dots & \dots & \dots & 0 & g \\ 0 & 0 & 0 & \dots & g & 0 \end{pmatrix}. \quad (\text{A2})$$

Since  $\mathbf{A}$  is symmetric, it can be diagonalized by an orthogonal transformation  $\mathbf{K}$ , i.e.,  $\mathbf{K}^T \mathbf{A} \mathbf{K} = \mathbf{D}$ , where  $\mathbf{D}$  is a diagonal matrix containing the eigenvalues  $\lambda_i$  of  $\mathbf{A}$ . Thus defining the new variables  $\mathbf{Q} = \mathbf{K}^T \mathbf{q}$  and  $\mathbf{P} = \mathbf{K}^T \mathbf{p}$ , we can rewrite the Hamiltonian as

$$H_E = \sum_{i=1}^N \left[ \frac{P_i^2}{2} + \frac{v_i^2 Q_i^2}{2} \right], \quad (\text{A3})$$

where the eigenfrequencies are  $v_i = \sqrt{2\lambda_i}$ , and again  $\mathbf{Q} \equiv \{Q_1, Q_2, \dots, Q_N\}^T$  and  $\mathbf{P} \equiv \{P_1, P_2, \dots, P_N\}^T$ . Thus we passed from a chain environment into the equivalent star model.

#### APPENDIX B: FULL DIAGONALIZATION AND TIME EVOLUTION

The starting point is the total Hamiltonian  $H = H_S + H_E + H_I$  after the diagonalization of the environment. Since  $H$  is also quadratic in position and momentum operators, it can again be written as

$$H = \frac{\mathbf{p}^T \mathbf{p}}{2} + \mathbf{q}^T \mathbf{B} \mathbf{q} \quad (\text{B1})$$

where, contrary to the notation of last section, we have  $\mathbf{q} \equiv \{q_1, q_2, \dots, q_N, q_S\}^T$  and  $\mathbf{p} \equiv \{p_1, p_2, \dots, p_N, p_S\}^T$ . The  $(N+1) \times (N+1)$  matrix  $\mathbf{B}$  has elements  $B_{ii} = v_i^2/2$  for  $i = 1, \dots, N$ ,  $B_{N+1, N+1} = \omega_S^2/2$ , and  $B_{i, N+1} = B_{N+1, i} = -\tilde{g}_i/2$ .

We can again perform a diagonalization of  $\mathbf{B}$  through an orthogonal matrix  $\mathbf{O}$ , i.e.,  $\mathbf{O}^T \mathbf{B} \mathbf{O} = \mathbf{F}$ , and upon defining the new system-environment normal modes  $\mathbf{Q} = \mathbf{O}^T \mathbf{q}$  and  $\mathbf{P} = \mathbf{O}^T \mathbf{p}$ , we rewrite the full Hamiltonian as

$$H = \sum_{i=1}^{N+1} \left[ \frac{P_i^2}{2} + \frac{f_i^2 Q_i^2}{2} \right], \quad (\text{B2})$$

where  $\sqrt{2}f_i$  are the eigenvalues of  $\mathbf{B}$  contained in the diagonal matrix  $\mathbf{F}$ .

In this picture, the time evolution for each normal mode is trivial,

$$Q_i(t) = Q_i(0) \cos(f_i t) + \frac{P_i(0)}{f_i} \sin(f_i t), \quad (\text{B3})$$

$$P_i(t) = -f_i Q_i(0) \sin(f_i t) + P_i(0) \cos(f_i t).$$

Now, remembering the new variables are connected to the old ones through the orthogonal transformation  $\mathbf{O}$  at any time  $t$ , we easily get

$$q_i(t) = \sum_{j=1}^{N+1} [\mathbf{B}_{ij}^{QQ}(t) q_j(0) + \mathbf{B}_{ij}^{QP}(t) p_j(0)], \quad (\text{B4})$$

$$p_i(t) = \sum_{j=1}^{N+1} [\mathbf{B}_{ij}^{PQ}(t) q_j(0) + \mathbf{B}_{ij}^{PP}(t) p_j(0)].$$

where

$$\begin{aligned} \mathbf{B}^{QQ}(t) &= \mathbf{O} \cdot \mathbf{C} \mathbf{o} \cdot \mathbf{O}^T, \\ \mathbf{B}^{QP}(t) &= \mathbf{O} \cdot \frac{\mathbf{S} \mathbf{i}}{\mathbf{f}} \cdot \mathbf{C}^T, \\ \mathbf{B}^{PQ}(t) &= -\mathbf{O} \cdot f \mathbf{S} \mathbf{i} \cdot \mathbf{O}^T, \\ \mathbf{B}^{PP}(t) &= \mathbf{O} \cdot \mathbf{C} \mathbf{o} \cdot \mathbf{O}^T, \end{aligned} \quad (\text{B5})$$

where  $\mathbf{C} \mathbf{o}$  is the diagonal matrix with  $\mathbf{C} \mathbf{o}_{ii} = \cos(f_i t)$ ,  $f \mathbf{S} \mathbf{i}$  is also diagonal such that  $f \mathbf{S} \mathbf{i}_{ii} = f_i \sin(f_i t)$ , and  $\frac{\mathbf{S} \mathbf{i}}{f}_{ii} = \sin(f_i t)/f_i$ . Equations (B4) provide the time evolution of the position and momentum operators for the system and the normal modes when their form at time zero is given.

#### APPENDIX C: NUMERICAL EVALUATION OF NM MEASURES

Both  $M_{\text{BLP}}$  and  $M_{\text{RHP}}$  measures are evaluated numerically considering Gaussian states. The simulations for  $M_{\text{RHP}}$  have

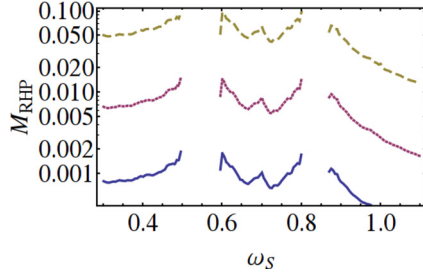


FIG. 6. (Color online) RHP non-Markovianity against system frequency  $\omega_S$  comparing the result with  $r = 1, 2, 3$  (continuous, dashed, dashed-dashed). The behavior is the same, only with higher absolute values. (Arbitrary units as specified in the caption of Fig. 1.)

been done for two-mode vacuum squeezed states between system and ancilla, with a squeezing parameter  $r = 1$  unless otherwise stated. As shown in Fig. 3 (extra black dot), increasing this parameter yields higher values for the measure. However, it is important to stress that there are no qualitative changes in the behavior of  $M_{\text{RHP}}$  (see Fig. 6).

The main issue with this measure is that for low system-bath couplings it is inconclusive (i.e.,  $M_{\text{RHP}} = 0$ ), but this can be easily fixed by increasing  $k$ . Typical time steps for integration of this measure  $\delta t = 0.1$  (e.g., for  $\tau_R \sim 700$  in Fig. 3) have been used, which is more than enough to resolve the positive slopes of the dynamics for  $E_{\text{SA}}$  [see Eq. (4)].

The simulations for  $M_{\text{BLP}}$  have been performed between pairs of one-mode vacuum squeezed states. As a finite set of states is considered our numerical analysis provides a lower bound for this measure. The possibility to evaluate  $M_{\text{BLP}}$  on a reduced family of (orthogonal) states [40] was recently reported but as we deal with Gaussian states—that are never orthogonal—we cannot restrict our analysis and we consider a number of Gaussian states as large as possible. We have checked that a further increase in the number of squeezed states does not significantly change our results. Interestingly, we actually see that in general “quasiorthogonal” squeezed states do not provide the best choice for the non-Markovianity maximizing pair. In Fig. 3 one of them has squeezing parameter  $r_1 = 1$  and phase-space angle  $\theta_1 = 0$  and for the other state  $r_2 \in [0.5, 1]$  with  $\Delta r_2 = 0.5$  and  $\theta_2 \in [0, \pi/2]$  with  $\Delta\theta_2 = \pi/4$  (same for Fig. 4 (right)); for Fig. 5 we have used  $r_2 \in [0.25, 1]$  with  $\Delta r_2 = 0.25$ ). The bold (blue) point in Fig. 3 in the main paper was obtained by increasing  $r_2 \in [0.125, 1.125]$ ,  $\Delta r_2 = 0.5$ , and  $\theta_2 \in [0, \pi/2]$  with  $\Delta\theta_2 =$

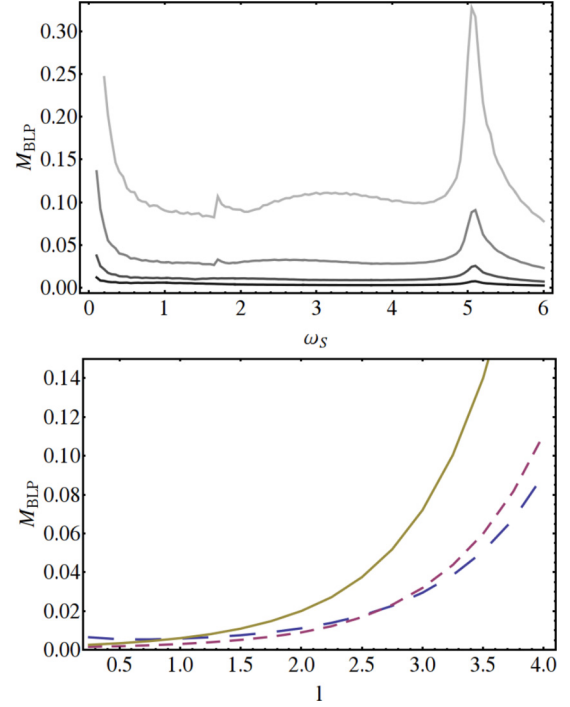


FIG. 8. (Color online) Top: BLP non-Markovianity against system frequency  $\omega_S$  with  $J(\omega) = k(\omega - \omega_0)^l \Theta(\omega_c - \omega)$ ,  $\omega_0 = 1$ ,  $\omega_c = 5$ ,  $k = 0.00001$ , and  $l = 1, 2, 3, 4$  (black for  $l = 1$  to gray for  $l = 4$ ). Bottom: BLP NM versus  $l$  evaluated at  $\omega_S = 1, 3, 5$  (sparse dashed, tight dashed, and continuous, respectively) for the spectral density above. (Arbitrary units as specified in the caption of Fig. 1.)

$\pi/4$ . Instead, for Fig. 4 (left and middle) we have used a much more thorough scan with  $r_1 = 1/3, 1, \theta_1 = 0, r_2 \in [0, 2]$ ,  $\Delta r_2 = 0.1$ , and  $\theta_2 \in [0, \pi]$  with  $\Delta\theta_2 = \pi/10$ . We stress that the behavior against temperature is quite sensitive to the range of squeezings used and needs to be scanned intensively, because the optimal pair for this measure depends on the bath temperature (mostly for low T). We show an example in Fig. 7.

#### APPENDIX D: NM BEHAVIOR WITH NON-OHMIC BATH FOR OTHER PARAMETRIZATIONS

The behavior of  $M_{\text{BLP}}$  under the non-Ohmic spectral density

$$J(\omega) = k(\omega/\omega_S)^l \Theta(\omega - 0.25) \Theta(0.75 - \omega) \quad (\text{D1})$$

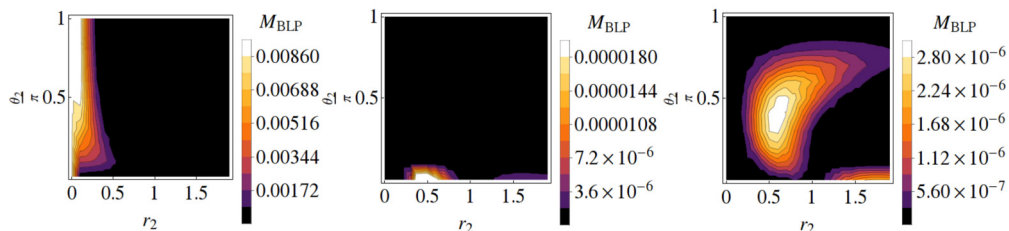


FIG. 7. (Color online) BLP non-Markovianity as used for the figures related to temperature, for  $T = 0, 0.5, 1$  and  $\omega_S = 0.375$  ( $r_1 = 1$ ). It can be seen that for higher temperatures several maxima appear at different squeezing parameters  $r_2, \theta_2$ . (Arbitrary units as specified in the caption of Fig. 1.)

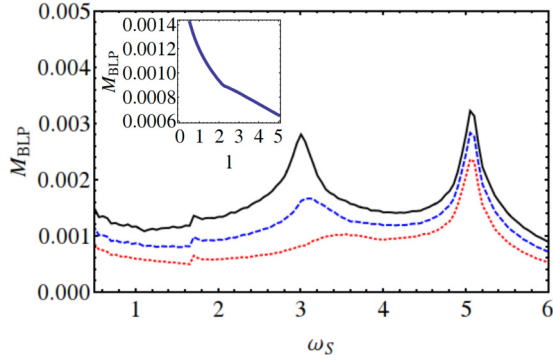


FIG. 9. (Color online) BLP non-Markovianity against system frequency  $\omega_S$  with  $J(\omega) = k[(\omega - \omega_0)/(\omega_c - \omega_0)]^l \Theta(\omega_c - \omega)$ ,  $\omega_0 = 3$ ,  $\omega_c = 5$ ,  $k = 0.0001$ , and  $l = 1/2, 1, 2$  (continuous, dashed, and dotted, respectively). We have drawn the spectral density to guide the eye. Inset: BLP NM versus  $l$  evaluated at  $\omega_S = 4$ . (Arbitrary units as specified in the caption of Fig. 1.)

was shown in Fig. 5. This is a spectral density which pivots around  $\omega_S$  and therefore keeps the coupling strength

at  $\omega_S$  [ $J(\omega_S) = k, \forall l$ ] fixed, while at the extreme points ( $\omega_0$  and  $\omega_c$ ) it differs in values. However, choosing for example

$$J(\omega) = k(\omega - \omega_0)^l \Theta(\omega_c - \omega) \quad (\text{D2})$$

[which keeps  $J(\omega_0)$  constant but differs at  $J(\omega_c)$  for different  $l$ ] would change the value of  $M_{\text{BLP}}$ , as shown in Fig. 8.

Deeper differences are found considering different power law spectra densities with constrained coupling strengths at both  $\omega_0$  and  $\omega_c$ , as results from

$$J(\omega) = k[(\omega - \omega_0)/(\omega_c - \omega_0)]^l \Theta(\omega_c - \omega) \quad (\text{D3})$$

[leading to  $J(\omega_0) = 0$  and  $J(\omega_c) = k, \forall l$ ]. In Fig. 9 it can be seen that the behavior of  $M_{\text{BLP}}$  is again different. It does actually decrease in the super-Ohmic case (larger  $l$  values).

We notice that in the latter two cases the spectral density at the system frequency  $J(\omega_S)$  differs in value when changing  $l$ , unlike the case discussed in Sec. V (star model). These examples show that normalization has to be carefully taken into account when drawing general conclusions about non-Markovian aspects of dissipation in the presence of different power laws in the spectral density.

- 
- [1] U. Weiss, *Quantum Dissipative Systems*, (World Scientific, Singapore, 2008); H.-P. Breuer and F. Petruccione, *The Theory of Open Quantum Systems* (Oxford University Press, New York, 2007); Gardiner and P. Zoller, *Quantum Noise* (Springer, Berlin 2004).
- [2] P. Hanggi and G.-L. Ingold, *Chaos* **15**, 026105 (2005).
- [3] S. John and T. Quang, *Phys. Rev. A* **50**, 1764 (1994).
- [4] H.-T. Tan, W.-M. Zhang, and G.-X. Li, *Phys. Rev. A* **83**, 062310 (2011).
- [5] J. Prior, I. de Vega, A. W. Chin, S. F. Huelga, and M. B. Plenio, *Phys. Rev. A* **87**, 013428 (2013).
- [6] U. Hoeppe, C. Wolff, J. Kuchenmeister, J. Niegemann, M. Drescher, H. Benner, and K. Busch, *Phys. Rev. Lett.* **108**, 043603 (2012).
- [7] D. A. Hite *et al.*, *Phys. Rev. Lett.* **109**, 103001 (2012).
- [8] S. Groblacher, A. Trubarov, N. Prigge, M. Aspelmeyer, and J. Eisert, [arXiv:1305.6942](https://arxiv.org/abs/1305.6942).
- [9] Bi-Heng Liu, Li Li, Yun-Feng Huang, Chuan-Feng Li, Guang-Can Guo, Elsi-Mari Laine, Heinz-Peter Breuer, and Jyrki Piilo, *Nat. Physics* **7**, 931 (2011).
- [10] W. M. Zhang, P. Y. Lo, H. N. Xiong, Matisse Wei-Yuan Tu, and F. Nori, *Phys. Rev. Lett.* **109**, 170402 (2012).
- [11] F. Haake and R. Reibold, *Phys. Rev. A* **32**, 2462 (1985).
- [12] B. L. Hu, J. P. Paz, and Y. Zhang, *Phys. Rev. D* **45**, 2843 (1992).
- [13] M. M. Wolf, J. Eisert, T. S. Cubitt, and J. I. Cirac, *Phys. Rev. Lett.* **101**, 150402 (2008).
- [14] H.-P. Breuer, E.-M. Laine, and J. Piilo, *Phys. Rev. Lett.* **103**, 210401 (2009).
- [15] A. Rivas, S. F. Huelga, and M. B. Plenio, *Phys. Rev. Lett.* **105**, 050403 (2010).
- [16] D. Chruściński and A. Kossakowski, *Phys. Rev. Lett.* **104**, 070406 (2010).
- [17] B. Bellomo, R. Lo Franco, and G. Compagno, *Phys. Rev. Lett.* **99**, 160502 (2007); A. W. Chin, S. F. Huelga, and M. B. Plenio, *ibid.* **109**, 233601 (2012); B. Bylicka, D. Chruściński, and S. Maniscalco, [arXiv:1301.2585](https://arxiv.org/abs/1301.2585).
- [18] M. B. Plenio, J. Hartley, and J. Eisert, *New J. Phys.* **6**, 36 (2004).
- [19] A. Wolf, G. De Chiara, E. Kajari, E. Lutz, and G. Morigi, *Europhys. Lett.* **95**, 60008 (2011).
- [20] E. Kajari, A. Wolf, E. Lutz, and G. Morigi, *Phys. Rev. A* **85**, 042318 (2012).
- [21] A. Rivas, A. D. K. Plato, S. F. Huelga, and M. B. Plenio, *New J. Phys.* **12**, 113032 (2010).
- [22] R. J. Rubin, *Phys. Rev.* **131**, 964 (1963), and references therein.
- [23] N. W. Ashcroft and N. D. Mermin, *Solid State Physics* (Saunders College, Philadelphia, 1976).
- [24] A. Walther, F. Ziesel, T. Ruster, S. T. Dawkins, K. Ott, M. Hettrich, K. Singer, F. Schmidt-Kaler, and U. Poschinger, *Phys. Rev. Lett.* **109**, 080501 (2012).
- [25] R. Bowler, J. Gaebler, Y. Lin, T. R. Tan, D. Hanneke, J. D. Jost, J. P. Home, D. Leibfried, and D. J. Wineland, *Phys. Rev. Lett.* **109**, 080502 (2012).
- [26] M. J. Hartmann, F. G. S. L. Brandao, and M. B. Plenio, *Laser Photon. Rev.* **2**, 527 (2008).
- [27] M. Aspelmeyer, S. Gröblacher, K. Hammerer, and N. Kiesel, *J. Opt. Soc. Am. B* **27**, A189 (2010).
- [28] Translation invariance of the environment is recovered by imposing an extra local potential to the first and last masses. This condition of homogeneous chain allows for a more immediate comparison with analytical results [23]. When  $g = h$  and  $\omega_0 = 0$ , in the limit  $N \rightarrow \infty$  a Rubin chain is recovered [22].
- [29] A rough estimate of the recurrence time can be given as the time it takes for the fastest phonon to travel back and forth along the chain. The group velocity of each phonon is simply  $v_k = dv_k/dk$ .

- [30] K. Życzkowski and I. Bengtsson, *Geometry of Quantum States* (Cambridge University Press, Cambridge, UK, 2008).
- [31] S. John and J. Wang, *Phys. Rev. Lett.* **64**, 2418 (1990).
- [32] R. Vasile, S. Maniscalco, M. G. A. Paris, H.-P. Breuer, and J. Piilo, *Phys. Rev. A* **84**, 052118 (2011).
- [33] In respect to the trace distance, the fidelity increases under any CP evolution.
- [34] D. Chruscinski, A. Kossakowski, and A. Rivas, *Phys. Rev. A* **83**, 052128 (2011); P. Haikka, J. D. Cresser, and S. Maniscalco, *ibid.* **83**, 012112 (2011).
- [35] A. W. Chin, A. Rivas, S. F. Huelga, and M. B. Plenio, *J. Math. Phys.* **51**, 092109 (2010).
- [36] R. Martinazzo, B. Vacchini, K. H. Hughes, and I. Burghardt, *J. Chem. Phys.* **134**, 011101 (2011).
- [37] P. Haikka, T. H. Johnson, and S. Maniscalco, *Phys. Rev. A* **87**, 010103 (2013).
- [38] G. Manzano, F. Galve, G. L. Giorgi, E. Hernández-García, and R. Zambrini, *Sci. Rep.* **3**, 1439 (2013).
- [39] T. J. G. Apollaro, C. Di Franco, F. Plastina, and M. Paternostro, *Phys. Rev. A* **83**, 032103 (2011).
- [40] S. Wissmann, A. Karlsson, E.-M. Laine, J. Piilo, and H.-P. Breuer, *Phys. Rev. A* **86**, 062108 (2012).